# Ultrafast to Ultraslow Dynamics of a Langmuir Monolayer at the Air/Water Interface Observed with Reflection Enhanced 2D IR Spectroscopy

Chang Yan, Joseph E. Thomaz, Yong-Lei Wang, Jun Nishida, Rongfeng Yuan, John P. Breen, and Michael D. Fayer*

Department of Chemistry, Stanford University, Stanford, California 94305, United States

S *Supporting Information*

ABSTRACT: Monolayers play important roles in naturally occurring phenomena and technological processes. Monolayers at the air/water interface have received considerable attention, yet it has proven difficult to measure monolayer and interfacial molecular dynamics. Here we employ a new technique, reflection enhanced two-dimensional infrared (2D IR) spectroscopy, on a carbonyl stretching mode of tricarbonylchloro-9-octadecylamino-4,5-diazafluorenerhenium(I) (TReF18) monolayers at two surface densities. Comparison to experiments on a water-soluble version of the metal carbonyl headgroup shows that water hydrogen bond rearrangement dynamics slow from 1.5 ps in bulk water to 3.1 ps for interfacial water. Longer time scale fluctuations were also observed and attributed to fluctuations of the number of hydrogen bonds formed between water and the three carbonyls of TReF18. At the higher surface density, two types of TReF18 minor structures are observed in addition to the main structure. The reflection method can take usable 2D IR spectra on the monolayer within 8 s, enabling us to track the fluctuating minor structures' appearance and disappearance on a tens of seconds time scale. 2D IR chemical exchange spectroscopy further shows these structures interconvert in 30 ps. Finally, 2D spectral line shape evolution reveals that it takes the monolayers hours to reach macroscopic structural equilibrium.
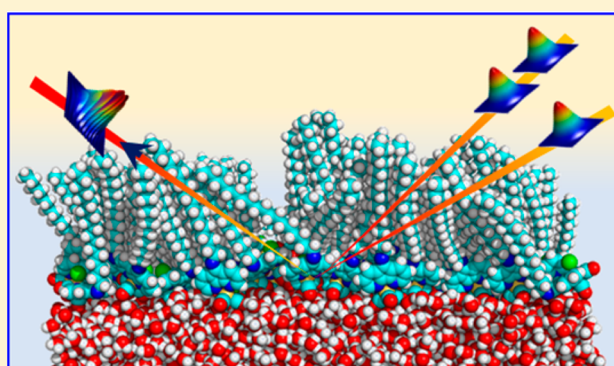
INTRODUCTION

On a water surface, a surfactant can spontaneously spread to form a molecular single layer: the Langmuir monolayer.[1] The Langmuir monolayers have been widely adopted as a model system for interfacial self-ordering, and phospholipid monolayers have often been used as models for biological membranes.[2,3] The two-dimensional (2D) organization in a Langmuir monolayer is sensitive to several controllable factors such as temperature, surface pressure, pH, and the surfactant chemical structure. The nonbulk molecular dynamics of interfacial water and surfactants in a model Langmuir monolayer provide important insights for understanding 2D phase transitions,[2,3] dynamics of biological water,[4] the solvation and conformational dynamics of proteins,[5] and mechanisms of trans-membrane activities.[6,7] Two-component Langmuir monolayers can contain metastable coexisting phase domains with a wide distribution of sizes and shapes that evolve on multiple time scales from minutes to weeks.[8,9] However, little information exists on how the ultrafast molecular dynamics and the extended time scale dynamics of the metastable structures are related.

Over the past few decades, the developments of many surface-selective techniques greatly expanded information on the time-averaged interfacial structures of Langmuir monolayers and on slowly evolving structures of multicomponent monolayers. Techniques include X-ray diffraction,[10] epifluorescence microscopy,[2] Brewster angle microscopy (BAM),[11] infrared reflection−absorption spectroscopy (IRRAS),[12] and steady-state vibrational sum frequency generation spectroscopy (VSFG).[13] Yet it is still challenging for optical spectroscopy to directly measure interfacial molecular dynamics on ultrafast time scales. The small number of chromophores in a single layer of molecules demands spectroscopic methods simultaneously possessing monolayer sensitivity as well as subpicosecond temporal resolution. Molecular dynamics simulations have provided important insights on the interfacial dynamics of water and surfactants,[3,14−16] yet robust experimental observables for comparison are lacking.

Two-dimensional infrared vibrational echo spectroscopy (2D IR) is an ultrafast third-order nonlinear optical method that measures structural dynamics because they generate vibrational frequency fluctuations.[17,18] 2D IR methods have been successfully applied for investigating hydrogen bond (H-

bond) rearrangements in aqueous[19,20] and organic solutions,[21] solvent dynamics in nanoconfined environments,[22] conformational fluctuations in biological macromolecules,[7,23] as well as many other types of systems. Two-dimensional heterodyne-detected vibrational sum frequency generation spectroscopy (2D HD-VSFG) has been implemented as an option to achieve interfacial selectivity.[24] It has been applied for studying interfacial water dynamics of Langmuir monolayers[25] and at the air/neat water interface[26] using the hydroxyls of water as the vibrational probe. However, the fourth-order 2D HD-VSFG requires vibrational modes that are both IR-active and Raman-active, and therefore the signal-to-noise (S/N) ratio is limited by its intrinsically low signal level.[27] Furthermore, such experiments provided little information on surfactant dynamics and typically do not span a broad time range.

The alternative to 2D HD-VSFG for the study of monolayers at the air/water interface or other monolayers that contain vibrational chromophores, is to directly apply 2D IR spectroscopy.[27] Because a monolayer only resides at the interface, it is unnecessary to have a surface specific technique. Monolayer vibrational chromophores with large infrared extinction coefficients and long vibrational relaxation lifetimes, such as metal carbonyls, can be used. These chromophores greatly improve the S/N ratio in the acquired 2D IR spectra.[27] The relatively long lifetime also enables detailed observation of interfacial dynamics over extended time periods of tens of picoseconds. The surface-specific labeling method has only been implemented in 2D IR measurements of solid/air and solid/solvent interfaces, that is, monolayers immobilized or adsorbed on silica,[28] gold,[29,30] and electrode surfaces,[31] which are fundamentally different from the more flexible and dynamical air/water interface.

Here we report the use of reflection geometry enhanced 2D IR[32] to investigate a Langmuir monolayer formed by a metal carbonyl surfactant, *fac*-tricarbonylchloro-9-octadecylamino-4,5-diazafluorenerhenium(I) (TReF18). 2D IR signals measured by advanced pump—probe pulse-shaping systems can be enhanced by a factor as great as 50 when applying the reflection geometry on dielectric interfaces.[32] The use of the reflection mode made possible 2D IR measurements of air/water interfacial monolayer dynamics with S/N ratios comparable to bulk solution samples. Moreover, the methodologies employed here can acquire 2D IR spectra with measurement times as short as 8 s, enabling real-time monitoring of structural evolution at the air/water interface over the course of hours.

■ EXPERIMENTAL METHODS

Sample Preparation. TReF18 was synthesized and purified by recrystallization using a previously reported method.[33] The dish and glassware used in the following monolayer deposition procedure were first cleaned with methanol, then with large amounts of deionized ultrafiltered water, and finally with large amounts of ultrapure water. To deposit a TReF18 monolayer for 2D IR or FT-IR measurements, ultrapure H_2O (resistance >18 MΩ cm, purchased from RICCA Chemical Company) was placed in a round Teflon Petri dish (diameter = 140 mm) until a slight meniscus was formed above the edge of the dish. Prior to monolayer deposition, the water surface was further cleaned by a vacuum aspirator. Then a predetermined volume of the 0.86 mg/mL TReF18 chloroform solution was spread on the clean water surface. The added volume was calculated such that the monolayer formed would reach the desired mean molecular area once the chloroform had evaporated. Using a Langmuir—Blodgett trough equipped with a microbalance for surface pressure measurements, we verified that the same surface pressure was reached for a certain mean

molecular area in the liquid expanded phase region, regardless of whether the monolayer was formed by directly adding TReF18 molecules to a fixed surface area or formed by compressing a lower density monolayer. We waited ~30 min for chloroform to completely evaporate before starting the measurements.

fac-Tricarbonylchloro-2,2′-bipyridine-4,4′-dicarboxylrhenium(I) was synthesized according to a published procedure.[34] The corresponding dilute ~1 mM aqueous solution of its sodium salt, referred as TReBDC, was prepared by dissolving the neutral complex in a D_2O/NaOH solution. The pH of the final solution was 12.3. The structures of TReF18 and TReBDC's anion are shown in Figure 1. [1]H
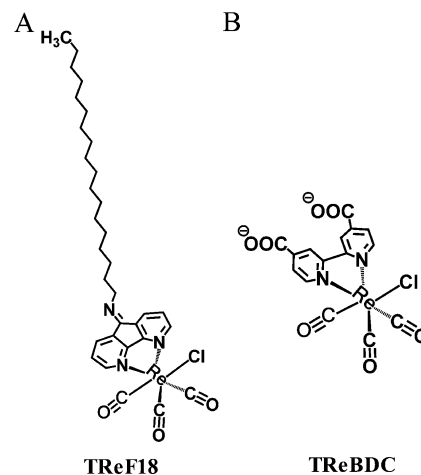
Figure 1. Molecular structures of TReF18 (A) and TReBDC anion (B).

nuclear magnetic resonance spectra and mass spectra data of TReF18 and TReBDC were used to confirm the identity of the synthesized molecules and are given in the Supporting Information.

Steady-State Measurements. Fourier transform infrared (FT-IR) absorption spectroscopy measurements of bulk solutions were performed on a Thermo Scientific Nicolet 6700 spectrometer equipped with a deuterated triglycine sulfate (DTGS) detector, and solution samples were placed between two 1-in. diameter calcium fluoride windows. All FT-IR spectra were recorded with 0.5 cm^{-1} resolution for 64 scans under dry CO_2-free atmosphere. Solvent and air absorption were subtracted as the background. IRRAS spectra of monolayers were collected on a Bruker Vertex 70 spectrometer with a liquid nitrogen cooled mercury cadmium telluride (MCT) detector. All monolayer spectra were collected using *s*-polarized IR beam at an incident angle of 50°. Each IRRAS spectrum was acquired at the resolution of 0.5 cm^{-1} for 1024 scans over the course of ~15 min. The background spectrum was taken on water surface before spreading the TReF18 monolayer on the surface. For the convenience of comparison to bulk spectra, the signs of absorbance of all the IRRAS spectra reported here were inverted.

A Biolin Scientific NIMA KN2002 Langmuir—Blodgett trough was used to collect the surface pressure—area isotherms at 21 °C. Ultrapure water (resistance >18 MΩ cm) was added to the cleaned trough until the water surface formed a meniscus ~1 mm above the lip of the Teflon trough. A platinum plate dipped into the water was used as the Wilhelmy plate for measuring surface pressure. A test isotherm was collected by compressing the Delrin barriers at a rate of 10 mm/min to ensure the absence of surface contaminations. Then TReF18 dissolved in chloroform at a concentration of 0.86 mg/mL was deposited over the water surface drop-by-drop through a glass microsyringe. Fifteen minutes were allowed for chloroform evaporation after which the barriers were compressed at a rate of 5 mm/min to obtain the isotherm curve.

2D IR Measurements. Mid-IR pulses with duration of ~160 fs, bandwidth of ~90 cm^{-1}, pulse energy ~30 μJ, and centered at 2025 cm^{-1} were generated at 3 kHz with an optical parametric amplifier

pumped by a regeneratively amplified Ti:sapphire laser system. The pulse frequencies selectively excited the carbonyl symmetric stretching mode of TReF18 without exciting other vibrational modes such as the two asymmetric stretch modes at ~1925 cm^{-1}. The frequencies chosen avoided the enormous water background in other regions without producing heating effect in the 2D IR spectra (see Supporting Information). The mid-IR beam was then split by a 10:90 beam splitter into the weak probe beam passing through a mechanical delay line and a strong pump beam passing through an acousto-optic modulator acting as the Fourier-domain pulse shaper.

The 2D IR experiments were conducted in a pump−probe geometry as the pulse shaper formed the pump pulse into 2 collinear pulses, denoted as pulses 1 and 2, with a variable delay, τ between them. The probe pulse, i.e. pulse 3, arrived after pulse 2 with the delay being the waiting time, T_w, controlled by the mechanical delay line. The pump and probe beams were focused to a diameter of ~120 μm and overlapped spatially at the sample with a crossing angle of 20°. The three pulses induced a third-order nonlinear polarization $P^{(3)}$ in the monolayer that emitted the vibrational echo pulse traveling collinearly with pulse 3. Pulse 3 served as the local oscillator (LO) to heterodyne detect the echo signal. The combined echo/LO pulse transmitted through sample or reflected off sample surface was passed into a spectrometer equipped with a 32-channel liquid nitrogen cooled MCT array detector. At each T_w, the delay τ was scanned to generate an interferogram for each ω_m (vertical axis) frequency pixel on the array detector. Each interferogram was then Fourier transformed to give the ω_τ axis (horizontal axis) in a 2D spectrum.

For the ~1 mM TReBDC bulk D$_2$O solution, transmission mode 2D IR measurements were performed. For TReF18 monolayers, reflection mode 2D IR was employed to achieve enhancement and avoid water background absorption. As the water surface is horizontal, an excitation setup bringing the beams down from the top was used. The pump and probe beams were focused and crossed precisely at the monolayer/water surface. The incident angle was set to 45° and s-polarization for reflection was utilized in both the pump and probe beams. In addition to the echo signal that propagates in the forward direction, for monolayers and thin films, an equal amplitude signal is emitted in the direction that pulse 3 is reflected from the surface.[32] The electric fields associated with the LO and the signal are L and S respectively. The intensity of the LO is L^2 and the intensity of the heterodyned signal that needs to be detected is 2LS. In the forward direction, L^2 ≫ 2LS, so the signal term (the modulation of L^2) is extremely difficult to detect against the background of L^2.[32] If the incoming third pulse intensity is reduced, both L and S go down by the same factor, and there is no improvement in the modulation amplitude of 2LS relative to L^2. However, in the reflected direction, S is the same as in the forward direction but only a small amount of L is reflected from the surface. Thus, 2LS is reduced, but L^2 is reduced far more, leading to enhanced detection of the very weak signals.[32]

To prevent water evaporation from changing the optical alignment and the meniscus shape during the experiments, the water level was precisely maintained via a feedback system (see Supporting Information). A surface height sensor system (laser beam reflected from the water surface into a quad detector) was used to control a stepper motor syringe pump to add water at the rate of evaporation.

Two types of sample compartments were used for collecting 2D IR data. In the first scheme, the Petri dish containing the water and monolayer was placed open to air in a laser optics room supplied with dust-free air. In the other scheme, the Petri dish was enclosed in a box constantly purged with a gentle flow of 99.999% (5.0 T) ultrapure nitrogen gas. The experiment results show essentially no difference between the two sample systems. The results demonstrate that the experiments over many hours were not influenced by possible surface contamination. A comparison of the measured ultraslow monolayer structural evolution using these two methods can be found in the Supporting Information. The room temperature is 23.5 °C. The water temperature is 21.2 °C for measurements conducted in air and 22.5 °C for measurements conducted in the sealed box purged with ultrapure nitrogen. The slight difference in temperature is caused by the

difference in the water evaporation rates caused by the difference in the humidity in the two sample configurations.

The 2D IR spectra were normalized contour plots where the bluest contour in each spectrum was the most negative signal, and the reddest contour was the most positive signal. Below the diagonal 0−1 transition peaks were the 1−2 transition peaks with the opposite signal sign. All the dynamical information of interest here such as the CLS curves were calculated on 0−1 peaks. Due to the phase inversion in the reflection geometry, the heterodyned reflection 2D IR signal has the opposite sign compared with the transmission mode signal. The peak volumes plotted in Figure 8A and 8B were extracted by summing the absolute values of signal amplitudes within a square spectral region assigned for each 2D peak. For the main peak, the region was a 10 cm^{-1} × 10 cm^{-1} square centered at 2031 cm^{-1}. For the blue and red minor peaks, the regions were 4 cm^{-1} × 4 cm^{-1} squares centered at 2039 and 2021 cm^{-1} respectively. The square sizes chosen were close to the fwhm's of the main or minor structures' linear absorption bands.

■ RESULTS AND DISCUSSIONS

Steady-State Measurements. In the Langmuir monolayer, the carbonyl ligands are in the interfacial water layer while the C18 chains extend into the air. The surface pressure−area isotherm of the Langmuir monolayer formed by TReF18, presented in Figure 2, agrees well with a previous report.[33] Two
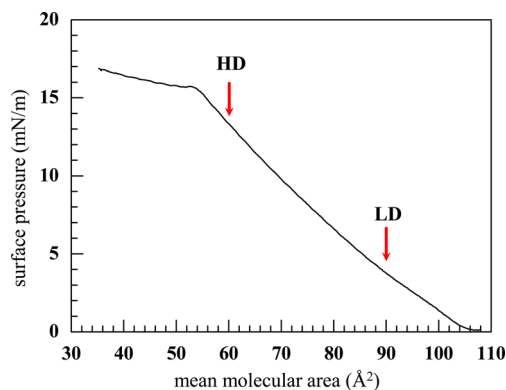
Figure 2. Surface pressure−area isotherm of TReF18. The locations of HD and LD monolayers on the isotherm are marked by red arrows.

surface densities were studied. The lower density (LD) monolayer had a mean molecular area of 90 Å^2 for each TReF18 molecule on the water surface, and the higher density (HD) monolayer had a mean area of 60 Å^2. Both the LD and HD monolayers are in the liquid expanded phase. The LD monolayer is near the low density end, while the HD monolayer is close to the transition between the liquid expanded phase and the liquid condensed phase.

The linear infrared absorption spectra of LD and HD monolayers are shown in Figure 3. The signal is exceedingly weak due to the small number of molecules in a monolayer. In Figure 3A, the LD monolayer spectrum contains a single peak for the carbonyl symmetric stretch mode centered at 2031.3 cm^{-1} with the full-width at half maxima (fwhm) of 12.8 cm^{-1}. The distortions of the red and blue side wings are caused by noise and imperfect background subtraction because of the low amplitude signals and the inability subtract background contributions from the monolayer itself. In contrast, the line shape of HD monolayer in Figure 3B was fit well by three distinct peaks. The major peak is at 2031.6 cm^{-1} with a fwhm of 12.9 cm^{-1}. These are the same within experimental error as the LD spectrum, which we refer to as the main structure peak. The other two narrower peaks at 2020.9 cm^{-1} (fwhm = 3.5 cm^{-1})
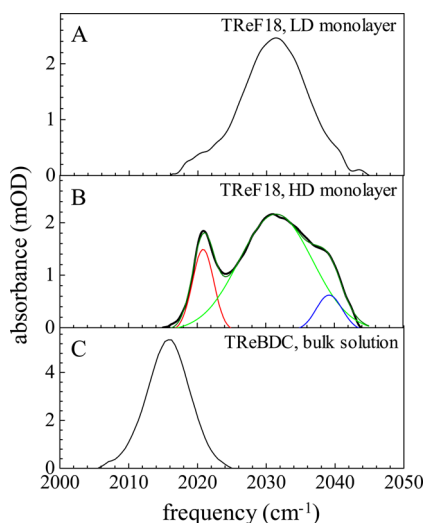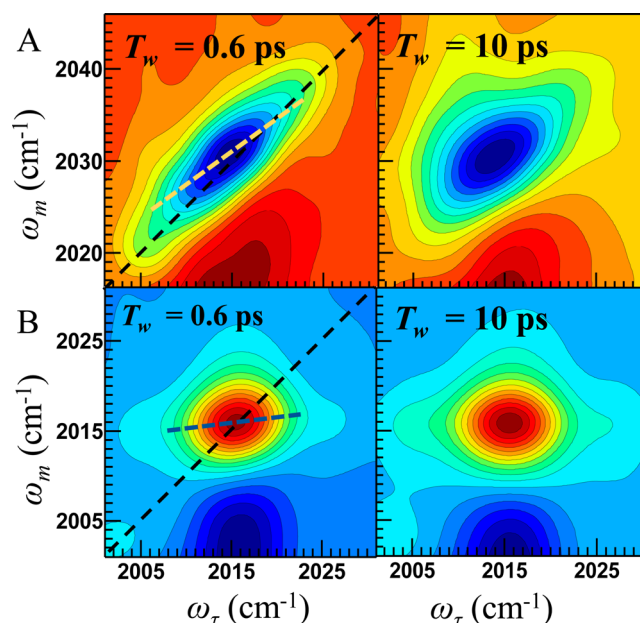
Figure 3. Linear absorption spectra of LD monolayer (A), HD monolayer (B), and ~1 mM TReBDC solution in D_2O (C). Black lines are the measured absorption lines. For the HD monolayer, the green line on top of the black line is the fit to the line shape composed of three Gaussians (main structure, light green; red minor structure, red; blue minor structure, blue).

Figure 4. (A) 2D IR spectra of LD monolayer at 0.6 ps (left) and 10 ps (right). (B) 2D IR spectra of ~1 mM TReBDC in Bulk D_2O solution at 0.6 ps (left) and 10 ps (right). The dashed yellow and blue lines are the center lines. Due to reflection mode method, the two spectra in A have the opposite signal sign from the transmission mode spectra of bulk sample in B.

and 2039.3 cm^{-1} (fwhm = 4.2 cm^{-1}) only appeared at high surface density or in high concentration bulk solutions in heptane/chloroform (see Supporting Information). We will refer to them as the red minor structure (lower frequency) and blue minor structure (higher frequency), respectively. The time-dependent spectral features of these bands will be discussed below with 2D IR results.

The linear IR absorption spectrum of the dilute TReBDC solution in D_2O is shown in Figure 3C. The peak is centered at 2016.0 cm^{-1} with a fwhm of 7.4 cm^{-1}. Quantum structure calculations showed that the red-shift relative to TReF18 is mainly caused by a small difference in the electron density of the carbonyls (see Supporting Information).

Ultrafast Interfacial Dynamics in LD Monolayer versus Bulk Dynamics. Principles of the 2D IR method have been summarized previously.[17,18] Qualitatively, 2D IR spectroscopy measures the structural dynamics of a system in the following manner. Molecules in different environments, e.g., different H-bond configurations, will give rise to different vibrational frequencies in the inhomogeneously broadened IR absorption spectrum. As the structure of the system evolves in time, the environments of the molecules causing the vibrational frequencies change. Therefore, measuring the time dependence of the frequencies, that is spectral diffusion, is a measurement of the time dependence of the structure. In the 2D IR experiment, the first two pulses label the molecules' initial frequencies (horizontal axis, ω_τ). The third pulse initiates a read out of the frequencies, and the detected echo pulse gives the final frequencies (vertical axis, ω_m). During the time T_w between the second and third pulses, the system's structure evolves. When T_w is short, there is little time for the structure to change, and the 2D spectrum is elongated along the diagonal (black dashed lines in Figure 4). As T_w is increased, the shape of the 2D spectrum changes, and the shape becomes more round. By analyzing the shape changes of a series of 2D spectra with increasing T_w, the time dependence of the structural dynamics is obtained. Examples of 2D spectra are given in Figure 4 at

short and long T_ws. Note the high quality of the 2D spectra taken on the monolayer (top panels).

The T_w dependent shapes of the 2D spectra were analyzed to determine the frequency-frequency correlation function (FFCF), which is obtained from the spectra using the center line slope (CLS) method.[35,36] The slope of a center line is the normalized FFCF at a certain T_w, and time-dependent plots are given in Figure 5. The CLS plots are modeled as a sum of exponentials. The FFCF also gives the homogeneous line width that arises from ultrafast processes that result in motional
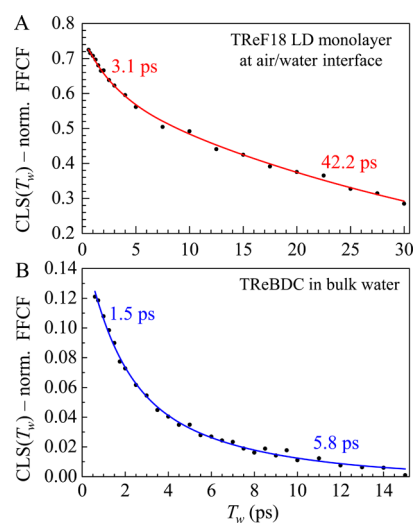
Figure 5. (A) LD monolayer CLS data (points) obtained from 2D IR spectra measured from 0.6 to 30 ps. (B) Bulk solution CLS data (points) obtained from 2D IR spectra measured from 0.6 to 15 ps. The solid curve in each panel is the biexponential fit. The numbers by the curves are the time constants.

narrowing. The homogeneous line contributes a Lorentzian component to the absorption spectrum. In the 2D spectra, the larger the contribution of homogeneous line width in the total absorption line width is, the closer to round (CLS value closer to zero) the spectrum will be at $T_w = 0$ ps. In the left-hand panels ($T_w = 0.6$ ps, very close to 0 ps) in Figure 4A and 4B, the spectrum from the bulk sample (TReBDC) is much closer to round than the monolayer spectrum (TReF18), showing the bulk sample has a much larger homogeneous line width. In other words, inhomogeneous broadening of the absorption band is more substantial at the interface than in the bulk solution.

In Figure 5 the CLS decays for the lower density (90 Å²) air/water interface monolayer (A) and the headgroup model in bulk water (B) are both fit very well with a biexponential decay function. The monolayer decay constants are 3.1 ± 0.5 ps and 42.2 ± 2.2 ps. In contrast, decay constants in the bulk water sample are 1.5 ± 0.2 ps and 5.8 ± 0.8 ps. Hydrogen bond dynamics in bulk H_2O and D_2O have been studied with 2D IR spectroscopy using the OD stretch of dilute HOD in H_2O and the OH stretch of dilute HOD in D_2O as the vibrational probes.[37−40] The 1.5 ± 0.2 ps decay of the FFCF was observed, and detailed simulations assigned this decay to the water hydrogen bond network randomization.[37,38] Simple anions[41,42] and metal carbonyls[43,44] used as 2D IR vibrational probes of water dynamics also reported the 1.5 ps decay. Hydrogen bond randomization involves the concert rearrangement of H-bonds. The frequency of a vibrational probe changes as the H-bonds undergo rearrangement because the frequency depends on the strength of the H-bonds. As discussed further below, water forms H-bonds to the carbonyls of TReF18 and TReBDC. Then, we assign the fast spectral diffusion time for TReBDC in bulk water as the water hydrogen bond network randomization time.

Both TReBDC in bulk water and the monolayer of TReF18 have biexponential decays of the CLS. The carbonyl regions of the two molecules are identical, except for a relatively small decrease in the electron density on the TReBDC carbonyls relative to the TReF18 carbonyls as shown by detailed electronic structure calculations. Therefore, we assign the fast 3.1 ps component of the CLS of TReF18 to water H-bond rearrangement and randomization in the interfacial water layer. H-bond rearrangement is a process that involves at least the first and second solvation shell around a vibrational probe.[40,45] In general, the number of H-bonds is maintained in the rearrangements, but H-bond partners switch in a concerted manner. The 2D IR results indicate that the H-bond rearrangement slows by approximately a factor of 2 at the air/water monolayer interface as compared to the bulk water solution. The slowing by a factor of ~2 is consistent with simulation results on air/water interface[15,16] and interfacial water dynamics at protein surfaces.[46] Similar slowing has been measured at water/solute interfaces in bulk solutions of proteins[43] and lipid membranes.[44]

The slow components of the spectral diffusion may also involve H-bond rearrangements, but the mechanism is different. There are three carbonyls in each TReF18 molecule. Atomistic simulations show that the carbonyl groups in TReF18 molecules can form various numbers of H-bonds with neighboring water molecules. The criteria used for identifying a hydrogen bond is that the O−O distance between a water oxygen and a carbonyl oxygen is less than 2.50 Å and the hydrogen bond angle is between 150° and 180°. As presented

in Figure 6A, the most probable configuration is one hydrogen bond to each carbonyl, for a total of 3 H-bonds. However, there
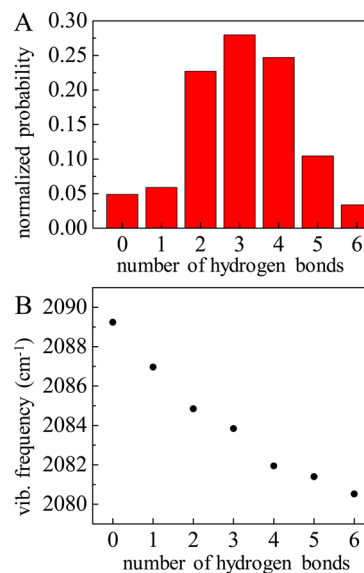
Figure 6. (A) Probability for TReF18 to form different numbers of hydrogen bonds with surrounding water molecules from MD simulations. (B) Dependence of the calculated tricarbonyl symmetric stretching mode frequency on the number of hydrogen bonds.

also can be 4 H-bonds, that is one of the carbonyls has two waters bound to it. There can be 2 H-bonds, where one of the carbonyls has no water molecule forming an H-bonds with it, as well as 5, 6, 1, and 0 H-bonds to the carbonyls. The probability of each H-bond number was calculated: 3 bonds −28%, 4 bonds −25%, and 2 bonds −23% (Figure 6A). The other four configurations have much lower probability, with these configurations sharing the remaining 24%. Representative structures consisting of one TReF18 molecule and six neighboring water molecules with H-bonds between carbonyls and water molecules were extracted from atomistic simulations and are shown in the Supporting Information.

These representative TReF18-water hydrogen bonding complex structures are further used as initial configurations to calculate the dependence of tricarbonyl symmetric stretching mode frequency on the number of hydrogen bonds through quantum chemical calculations. For each number of H-bonds to the carbonyls, a representative cluster of one TReF18 and six water molecules is taken from the simulation. The quantum calculation optimizes the structure, which only resulted in small changes from the initial cluster configuration obtained from the simulation. The quantum calculations provide the vibrational frequencies.

As displayed in Figure 6B, the quantum chemical calculations show that a larger number of H-bonds to the carbonyls shifts the symmetric CO stretching mode to lower frequency. The total range in the calculated frequencies is ~10 cm⁻¹ from 0 H-bonds to 6 H-bonds. The fwhm of the absorption line is 12.8 cm⁻¹ (see Figure 3A). Therefore, the various H-bond number configurations will be within the inhomogeneously broadened line, and will not appear as separate peaks. The detail procedures for the atomistic simulations that determined the representative H-bonding structures, and the subsequent quantum chemical calculations for determining carbonyl vibrational frequencies of these representative configurations

extracted from atomistic simulations are provided in the Supporting Information.

We assign the slow component in the CLS decays of TReF18 and TReBDC to fluctuations in the H-bond number. H-bond randomization preserves the number of H-bonds in the water. Except for brief transients at the transition state of the concerted H-bond rearrangement, a water molecule will have 4 H-bonds.[20] However, when the number of H-bonds to the carbonyls changes from 3 to 4, the water H-bond network must lose an H-bond. When the number changes from 3 to 2, the water network has an extra H-bond. Such processes should be unfavorable, and the water H-bond network may take a relatively long time to reach configurations that allow the number fluctuations. This process is considerably faster for the TReBDC in bulk water (5.8 ps) than it is for TReF18 at the air/water interface (42.2 ps). In bulk water, there is a three-dimensional H-bond network that may be able to more readily accommodate the number fluctuations than the restricted H-bond network in the interfacial layer. Furthermore, H-bond number fluctuations at the interface may involve coupling to structural dynamics in alkyl chain conformations of the monolayer, which have been observed on the time scale of tens of picoseconds for monolayers deposited on solid substrates.[29,47]

Multi-Time-Scale Evolution of the Metastable Structures in the Monolayer. In contrast to the low density monolayer (Figure 3A), the high density monolayer contained three peaks in the same frequency region as shown in the absorption spectrum (Figure 3B). The absorption spectrum was acquired over 15 min. However, we acquired 2D IR spectra with the waiting time fixed at T_w = 0.6 ps every 8.4 s for 700 min. While these very rapidly acquired spectra had substantial noise, the S/N ratio was sufficient to observe the peaks in the spectra. It was found that the number and types of peaks fluctuated with time. The spectra were sorted by peaks and the same type spectra were averaged to give good S/N. The results are shown in Figure 7A. The peaks are at the following frequencies, red minor structure 2020.9 cm^{-1}, main structure 2031.6 cm^{-1} and blue minor structure 2039.3 cm^{-1}. There are 4 distinct types of spectra. At some instants only the main structure band is present (Type I), at others only the main structure and the red minor structure are observed (Type II), at others the main structure and the blue minor structure are present (Type III), and at still other instants, all three bands are present (Type IV). While the main structure is always present, the minor structures come and go. Time independent spectra of TReBDC deposited on a TiO$_2$ surface with multiple peaks have been observed.[48] The air/water monolayer experiments were conducted on a macroscopic beam spot of ∼100 μm in radius. For the minor structure bands in the 2D IR spectra to appear and disappear, the structure of the monolayer over this macroscopic dimension must be fluctuating on a tens of seconds time scale. Some monolayer structures only permit the main structure to be present, while other structures make it possible for one minor structure or the other or both minor structures to form.

In addition to the macroscopic fluctuations, the minor structures are also forming and dissipating in tens of picoseconds. Figure 7B shows spectra measured at several T_ws with the main structure and both minor structures present. As T_w increases, off-diagonal peaks grow in. The off-diagonal corners of the black squares in the lower right-hand panel indicate the locations of the off diagonal peaks caused by
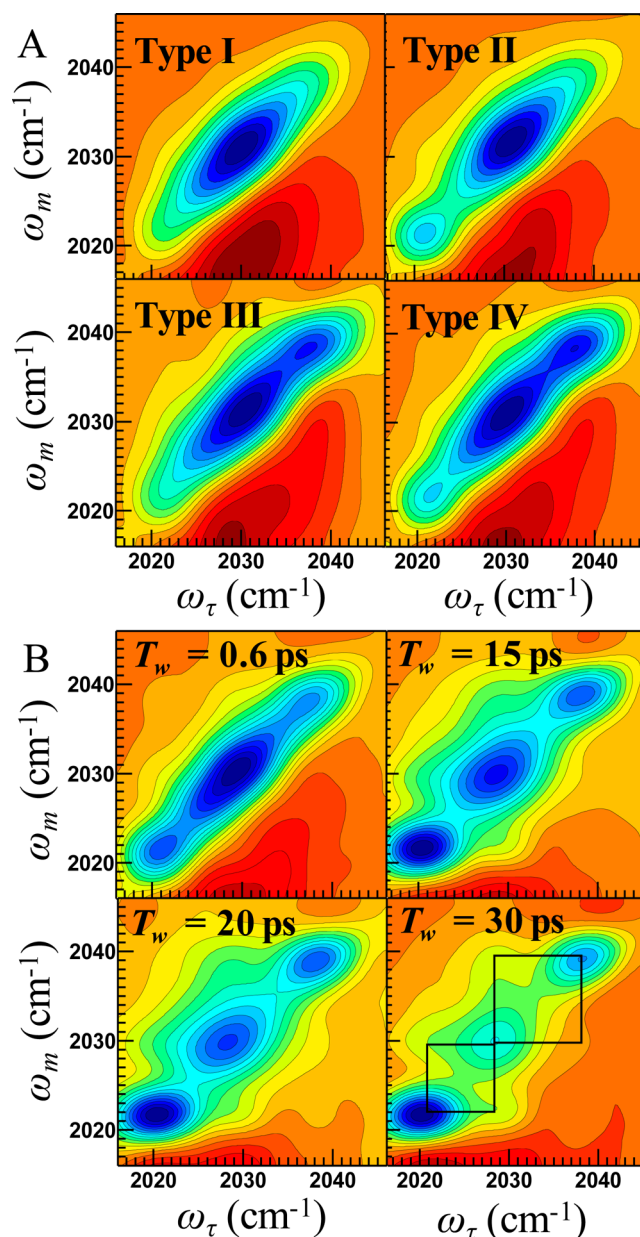

Figure 7. (A) The 2D IR spectra of the four spectral types I–IV at T_w = 0.6 ps observed in HD monolayer. (B) 2D IR spectra of HD monolayer measured at four T_ws. The off-diagonal peaks grow in. The corners of the black squares in the T_w = 30 ps panel mark the locations of the off-diagonal chemical exchange peaks.

ultrafast chemical exchange.[21,49] The off-diagonal peaks were observed regardless of whether only one or both of the minor structures were present. The minor structures were only observed in HD monolayers. The higher density enables the monolayer to undergo configurational fluctuations that permit the formation of structures giving rise to the minor structure bands. For the fraction of the monolayer that can form the minor structures, there is a rapid equilibrium, that is, Main ⇌ Minor. In the 2D spectra at T_w = 30 ps, the off-diagonal peaks have gain substantial amplitude in comparison to the diagonal peaks. A rough estimate of the time constants for exchange among the main and minor structures is ∼30 ps. The overall result is that while the macroscopic structure fluctuates on a tens of seconds time scale, enabling or disabling the formation of minor structures, when the minor structures are present,

molecular level ultrafast structural fluctuations produce formation and dissolution of minor structures in ~30 ps.

It is important to consider the possibility that vibrational excitation transfer between headgroups rather than structural chemical exchange causes the appearance of the off-diagonal peaks. Previous studies have shown that the rhenium carbonyl headgroups anchored on solid substrates with surface density substantially higher than the Langmuir monolayers studied here have very slow vibrational excitation transfer rates of ~800 ps.[50] A study of varying headgroup density on the silica substrate samples showed that excitation transfer did not occur.[51] Therefore, excitation transfer in the monolayers studied here is not responsible for the chemical exchange peaks.

We obtained detail information on the time-dependent appearance and disappearance of the minor structures. The volumes of the three diagonal peaks in each of the more than 5000 fast scans in 700 min were analyzed. Taking a spectrum every ~8 s, we are able to determine the presence or absence of each peak and determine if the spectrum is type I, II, III, or IV. Assuming that the infrared extinction coefficients of the three peaks are similar, the peak volumes at $T_w = 0.6$ ps reflect the population of the main structure and the two minor structures. Some characteristic scans are displayed in Figure 8A and 8B.
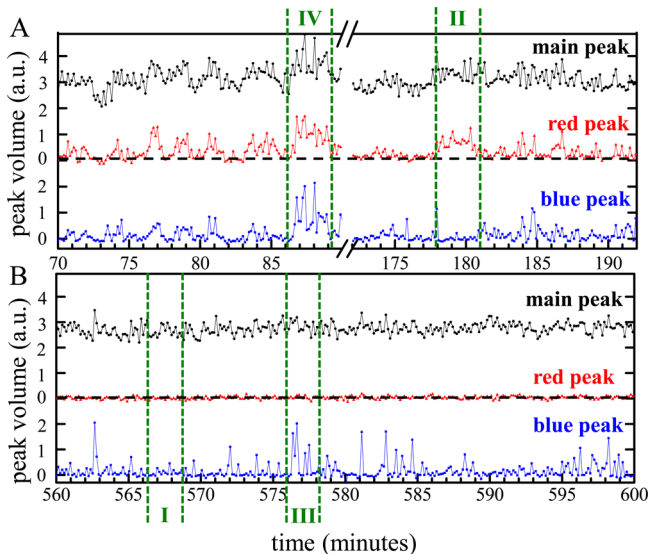
Figure 8. Volumes of the main structure peak, the red minor structure peak and the blue minor structure peak at $T_w = 0.6$ ps obtained from the fast 8-s scans within selected time ranges. The characteristic volume pattern for each spectral type I−IV is marked by the dashed green lines. The data for the blue minor structure are displaced downward and have their own vertical axis so they are not on top of the red minor structure data. (A) Data from 70 to 192 min. The main structure peak is always present, but the blue and red minor structure peaks appear and disappear. (B) Data from 560 to 600 min. The main structure peak is always present. The blue minor structure peak appears and disappears, but the red minor structure peak no longer appears.

The main structure (black) is always present and has an average value of ~3 in arbitrary units, but its amplitude fluctuates to some extent. In contrast, there are time periods during which the red or blue minor structures or both are not present. Therefore, only a fraction of the macroscopic laser spot at a given instant has structures that permit formation of the minor structures; only a fraction of the main structure band is

interconverting with the minor structure bands. In Figure 8A and 8B, green dashed lines bracket some typical time spans when the four types of spectra shown in Figure 7A occur. It should be noted that the fast fluctuations cannot be caused by thermal gradients associated with laser pulse heating the water. In the Supporting Information, we included an estimation which shows that the temperature within the laser spot is ~6 °C higher than the water outside of the spot, and the temperature gradient was stabilized within ~10 laser shots. As the laser repetition rate and intensity are constant, the temperature is also constant. Therefore, temperature fluctuations are not responsible structural fluctuations among types I−IV that persist for hours.

The existence of domains with different structures in Langmuir monolayers has been observed with epifluorescence microscopy when there is coexistence of liquid expanded phase and liquid condensed phase domains or when the monolayer is constituted by a binary mixture of two surfactants.[2,8,52,53] In these experiments, a low concentration fluorescent dye is doped into the monolayer. The concentrations of the dye in domains with different structures are different and therefore give a contrast image that shows the boundaries of domains. The domain diameters observed are ~100 μm, and the domain shape can keep evolving for a long period of time from days to weeks.[2,8] In the liquid expanded phase, the surfactant molecules are considered to lack ordering and show conformational flexibility of alkyl chains. In contrast, the liquid condensed phase has more ordered packing of surfactants and there can be multiple different liquid condensed phase structures.[52]

The HD monolayer has a surface density close to the phase transition point. One possibility is that the HD monolayer may contain some domains that have already nucleated into liquid condensed phase structures showing the blue and red minor peaks, while most of the surfactants are still in the liquid expanded phase domains represented by the major peak. However, the 2D IR experiments acquire vibrational spectroscopic signals rather than images of monolayer domains. The fluctuations of type I−IV signals observed in the ~100 μm laser spot on the HD monolayer surface demonstrate the existence of different structures but do not correspond to the same type of domain structures that have been observed with the epifluorescence microscopy. The chemical exchange cross peaks (see Figure 7B) reveal that the major and minor structures interchange on an ultrafast time scale, which is fundamentally distinct from the slow shape evolution governed by interdomain diffusion of surfactant molecules. In addition, the appearance and disappearance of the minor structures on a tens of seconds time scale (see Figure 8), is also inconsistent with interdomain diffusion of surfactant molecules.

Figure 8B shows a remarkable difference from Figure 8A. The red minor structure no longer occurs. The time span in Figure 8B covers from 9.3 to 10 h. In fact, the red minor structure ceases to appear after ~5 h. Then, in addition to monolayer structural fluctuations that cause the red and blue minor structures to appear and disappear, there is a much longer time scale evolution of the macroscopic structure of the monolayer. Configurations that permitted the formation of the red minor structure cease to exist after many hours.

To further examine the time-dependent evolving structures of both the HD and LD samples, in Figure 9A the shapes of the 2D spectra were tracked by determining the CLS over 15 h for the single $T_w = 0.6$ ps. A change in the CLS quantifies the change in the 2D band shape. The shapes of the spectra are
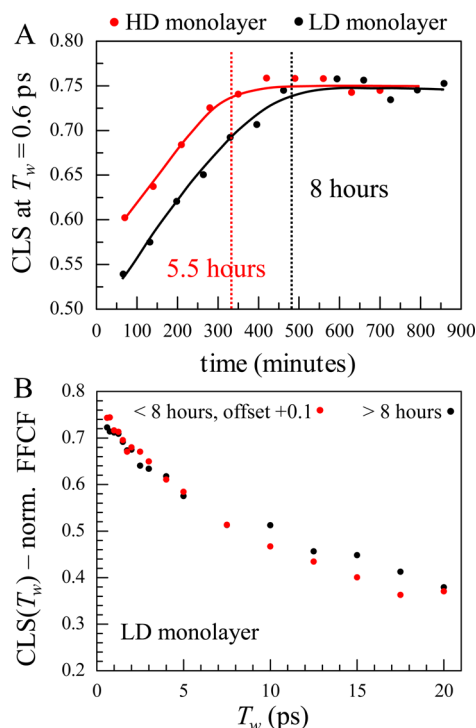
Figure 9. (A) The CLS values at T_w = 0.6 ps obtained from 2D IR spectra acquired from 60 to 850 min after monolayer deposition. Solid lines were drawn through data points to show the trend of structural evolution. The dashed lines mark the knees of structural evolution. (B) The CLS decay curve acquired in the first 8 h in comparison with the curve acquired in 8−14 h after the LD monolayer deposition. The CLS values in the early-time curve were offset by +0.1 to show that the decay curve shape (spectral diffusion) is the same within experimental error as that of the late-time curve.

determined by the structural fluctuations of the sample. At a single T_w, a change in shape means that there is a change in dynamics, which can only change if the macroscopic structure of the system has evolved. The dashed lines in Figure 9A are guide lines to indicate the knees of the time dependence. For both the HD and LD monolayers, the dynamics and therefore the monolayers' structures, are changing over many hours before the CLS values approach a constant value within the experimental error. These results show that either the structural evolution has come to completion or has become so slow that is not detectable within the experimental uncertainty. For the HD monolayer, the knee is at ∼5.5 h while for the LD monolayer it is at ∼8 h. An important observation is that the structures of both the HD and LD monolayers evolve over many hours. As discussed above and in detail in the Supporting Information, the long-term changes in the observed dynamics are not caused by slow contamination of the monolayer surface.

It was found that the spectral diffusion dynamics (decay time constants) did not change when CLS decay curves were compared at different times after the monolayer deposition. Only the homogeneous component of the line shape changed with time. As discussed above, the homogeneous component is manifested in the CLS plot as the curve's initial value at T_w = 0 ps. As shown in Figure 9A, the homogeneous line width decreases with time as shown by the difference between initial value at T_w = 0 ps and unity becomes smaller. The CLS decay curve does not change shape, but the entire curve moves up when a CLS decay measured at later times after monolayer

deposition is compared to a decay measured at earlier times. In Figure 9B, the CLS decay curve acquired in the first 8 h after monolayer deposition and the curve acquired during 8−14 h after deposition are shown. The early-time curve has been shifted up by 0.1 to account for the change in the homogeneous line width. With the shift the curves are essentially the same within experimental error.

Spectral diffusion is caused by structural fluctuations on the picosecond to tens of picosecond time scales. Both the time constants (τ, rate of frequency sampling) and amplitudes (Δ, range of the frequencies sampled) of the inhomogeneous Gaussian contributions to the absorption spectrum can be determined. In contrast, the homogeneous contribution to the spectrum is caused by ultrafast structural fluctuations, typically <100 fs,[40,41,54] that produce a motionally narrowed Lorentzian line shape contribution to the total absorption line. A contribution is motionally narrowed when $\Delta\tau < 1$, and it is not possible to determine Δ and τ separately. The homogeneous line width (Γ) is given by $\Gamma = \Delta^2\tau$. The points in Figure 9A are increasing in amplitude as time increases, suggesting that Γ is becoming narrower. The homogeneous line becoming narrower can be caused by τ becoming faster, Δ becoming smaller, or a combination of changes in Δ and τ such that their product becomes smaller. A likely possibility is that the range of frequencies (range of structures) is reduced. We observed that after many hours, the red minor structures no long occur, which shows that as time progresses, structures present at shorter times are not present at long time.

Small changes in the homogeneous contribution to the Voigt absorption line shape are difficult to track with linear absorption spectroscopy, particularly when the line is substantially inhomogeneously broadened, as is the case here. The 2D spectral analysis is much more sensitive to line shape change than linear IRRAS spectra because in 2D spectroscopy the homogeneous contribution is a distinct observable rather than a small contribution to the total absorption line shape. The 2D IR signals are also free from background absorption. Therefore, the 2D IR spectra were able to track the time evolution of the monolayer that would be problematic with absorption spectroscopy.

The time evolution of the monolayers' structures over many hours is remarkable. One way to consider this phenomenon qualitatively is in analogy to an MD simulation. In an MD simulation there is an "equilibration run" for a significant amount of time before the "production run", from which structural and dynamical information is obtained. In a simulation, the initial system is prepared with the molecules with realistic intermolecular potentials and therefore the correct forces acting on the molecules. However, the simulation is initiated with the molecules in arbitrary configurations, i.e., separations, orientations, etc. During the equilibration run, the time dependent forces act on the molecules until the equilibrium structure is obtained. Structural dynamics continue to occur, but these dynamics take place within the overall equilibrium structural ensemble. In the monolayer samples, as is the standard procedure,[33] the TReF18 is dissolved in chloroform and deposited on the surface. The chloroform evaporates in a few minutes, leaving the monolayer at the air/water interface. It seems reasonable that the initial config-urations of the molecules once the chloroform evaporates are not in the final monolayer equilibrium configurations. The results show (Figure 9A) that the macroscopic monolayer evolves over many hours.

The experiments were carried out in a clean laser room with controlled dust-free atmosphere. As discussed above and in the Supporting Information, the experiments were conducted with two types of sample systems, i.e., the monolayer was exposed to room air or the experiments were carried out in a seal container with an ultrapure nitrogen purge. With both sample systems, we observed the seconds-to-minutes fluctuations of the signal types I−IV shown in Figure 8. With both sample systems, the red minor structures ceased to exist after 5−6 h, and the CLS value of the major structure evolved over many hours (see Supporting Information). Therefore, the ultraslow dynamics observed in the TReF18 Langmuir monolayers originate from intrinsic monolayer structural changes rather than a slow buildup of contaminants.

■ CONCLUDING REMARKS

Ultrafast 2D IR vibrational spectroscopy has been applied to a monolayer at the air/water interface. Use of the new surface reflection geometry method provided the sensitivity to obtain high quality data that could be taken very rapidly. By comparing the spectral diffusion dynamics measured on the metal carbonyl vibrational probe headgroup at the air/water interface to an equivalent water-soluble version of the headgroup, it was found that the water H-bond structural randomization time, which involves concerted H-bond formation and dissociation, is approximately a factor of 2 slower in the interfacial water layer in contact with the monolayer. Another form of hydrogen bond dynamics, the fluctuation of the number of hydrogen bonds formed between water and the metal tricarbonyls, produced slower dynamics, which were significantly slower in the interfacial water layer than in bulk water.

Observations on a high surface density monolayer showed the presence of two types of minor structures in addition to the main structure species observed in the lower density monolayer. The minor structure species appeared and disappeared on a tens of seconds time scale, demonstrating that there were substantial fluctuations in the macrostructure of the monolayers. Chemical exchange cross peaks also showed that the main structure and minor structures interconvert on the ultrafast time scale of ∼30 ps. Detailed 2D IR data, taken over 15 h, revealed that the monolayer structures evolved over many hours after deposition on the water surface. The slow time for equilibration for a surfactant monolayer at the air/water interface may have implications for a wide variety of systems. For example, the breaking of ocean waves generates aerosol water droplets that can be coated with a monolayer of surfactants, like the monolayer studied here.[55] This surfactant layer may have a time-evolving structure that could influence the droplet properties and processes that occur in the aerosols.

■ ASSOCIATED CONTENT

Ⓢ Supporting Information

The Supporting Information is available free of charge on the ACS Publications website at DOI: 10.1021/jacs.7b06602.

> Characterization of the rhenium diimine complexes, description of the water level control system, details of MD simulations and quantum chemical calculations, FT-IR spectra of a TReF18 oversaturated bulk solution, background 2D IR spectra of LD monolayer measured at T_w = −100 and 100 ps, comparison of ultraslow dynamics measured in dust-free room air versus in an ultrapure nitrogen atmosphere, and discussions of water heating due to the IR pulses (PDF)

■ AUTHOR INFORMATION

Corresponding Author
*fayer@stanford.edu

ORCID Ⓞ
Chang Yan: 0000-0001-9735-3002
Yong-Lei Wang: 0000-0003-3393-7257
Jun Nishida: 0000-0001-7834-8179
Michael D. Fayer: 0000-0002-0021-1815

Notes
The authors declare no competing financial interest.

■ REFERENCES

(1) Langmuir, I. *J. Am. Chem. Soc.* **1917**, *39*, 1848−1906.
(2) McConnell, H. M. *Annu. Rev. Phys. Chem.* **1991**, *42*, 171−195.
(3) Kaganer, V. M.; Möhwald, H.; Dutta, P. *Rev. Mod. Phys.* **1999**, *71*, 779−819.
(4) Bagchi, B. *Chem. Rev.* **2005**, *105*, 3197−3219.
(5) Pratt, L. R.; Pohorille, A. *Chem. Rev.* **2002**, *102*, 2671−2691.
(6) Branden, M.; Sanden, T.; Brzezinski, P.; Widengren, J. *Proc. Natl. Acad. Sci. U. S. A.* **2006**, *103*, 19766−19770.
(7) Mukherjee, P.; Kass, I.; Arkin, I. T.; Zanni, M. T. *Proc. Natl. Acad. Sci. U. S. A.* **2006**, *103*, 3528−3533.
(8) McConnell, H. M. *Proc. Natl. Acad. Sci. U. S. A.* **1996**, *93*, 15001−15003.
(9) Seul, M.; Andelman, D. *Science* **1995**, *267*, 476−483.
(10) Kjaer, K.; Alsnielsen, J.; Helm, C. A.; Laxhuber, L. A.; Möhwald, H. *Phys. Rev. Lett.* **1987**, *58*, 2224−2227.
(11) Henon, S.; Meunier, J. *Rev. Sci. Instrum.* **1991**, *62*, 936−939.
(12) Dluhy, R. A.; Cornell, D. G. *J. Phys. Chem.* **1985**, *89*, 3195−3197.
(13) Shen, Y. R. *Annu. Rev. Phys. Chem.* **2013**, *64*, 129−150.
(14) Lopez, C. F.; Nielsen, S. O.; Klein, M. L.; Moore, P. B. *J. Phys. Chem. B* **2004**, *108*, 6603−6610.
(15) Ni, Y. C.; Gruenbaum, S. M.; Skinner, J. L. *Proc. Natl. Acad. Sci. U. S. A.* **2013**, *110*, 1992−1998.
(16) Roy, S.; Gruenbaum, S. M.; Skinner, J. L. *J. Chem. Phys.* **2014**, *141*, 22D505.
(17) Hamm, P.; Zanni, M. T. *Concepts and Methods of 2D Infrared Spectroscopy*; Cambridge University Press: Cambridge, 2011.
(18) Park, S.; Kwak, K.; Fayer, M. D. *Laser Phys. Lett.* **2007**, *4*, 704−718.

(19) Ji, M. B.; Odelius, M.; Gaffney, K. J. *Science* **2010**, *328*, 1003−1005.

(20) Eaves, J. D.; Loparo, J. J.; Fecko, C. J.; Roberts, S. T.; Tokmakoff, A.; Geissler, P. L. *Proc. Natl. Acad. Sci. U. S. A.* **2005**, *102*, 13019−13022.

(21) Zheng, J.; Kwak, K.; Asbury, J. B.; Chen, X.; Piletic, I. R.; Fayer, M. D. *Science* **2005**, *309*, 1338−1343.

(22) Roy, S.; Skoff, D.; Perroni, D. V.; Mondal, J.; Yethiraj, A.; Mahanthappa, M. K.; Zanni, M. T.; Skinner, J. L. *J. Am. Chem. Soc.* **2016**, *138*, 2472−2475.

(23) Kim, Y. S.; Hochstrasser, R. M. *J. Phys. Chem. B* **2009**, *113*, 8231−8251.

(24) Nihonyanagi, S.; Yamaguchi, S.; Tahara, T. *Chem. Rev.* **2017**, *117*, 10665−10693.

(25) Singh, P. C.; Inoue, K.; Nihonyanagi, S.; Yamaguchi, S.; Tahara, T. *Angew. Chem., Int. Ed.* **2016**, *55*, 10621−10625.

(26) Hsieh, C. S.; Okuno, M.; Hunger, J.; Backus, E. H. G.; Nagata, Y.; Bonn, M. *Angew. Chem., Int. Ed.* **2014**, *53*, 8146−8149.

(27) Kraack, J. P.; Hamm, P. *Chem. Rev.* **2017**, *117*, 10623−10664.

(28) Rosenfeld, D. E.; Gengeliczki, Z.; Smith, B. J.; Stack, T. D. P.; Fayer, M. D. *Science* **2011**, *334*, 634−639.

(29) Yan, C.; Yuan, R.; Pfalzgraff, W. C.; Nishida, J.; Wang, L.; Markland, T. E.; Fayer, M. D. *Proc. Natl. Acad. Sci. U. S. A.* **2016**, *113*, 4929−4934.

(30) Kraack, J. P.; Lotti, D.; Hamm, P. *J. Chem. Phys.* **2015**, *142*, 212413.

(31) Lotti, D.; Hamm, P.; Kraack, J. P. *J. Phys. Chem. C* **2016**, *120*, 2883−2892.

(32) Nishida, J.; Yan, C.; Fayer, M. D. *J. Chem. Phys.* **2017**, *146*, 094201.

(33) Yam, V. W. W.; Wang, K. Z.; Wang, C. R.; Yang, Y.; Cheung, K. K. *Organometallics* **1998**, *17*, 2440−2446.

(34) Smieja, J. M.; Kubiak, C. P. *Inorg. Chem.* **2010**, *49*, 9283−9289.

(35) Kwak, K.; Park, S.; Finkelstein, I. J.; Fayer, M. D. *J. Chem. Phys.* **2007**, *127*, 124503.

(36) Kwak, K.; Rosenfeld, D. E.; Fayer, M. D. *J. Chem. Phys.* **2008**, *128*, 204505.

(37) Asbury, J. B.; Steinel, T.; Kwak, K.; Corcelli, S. A.; Lawrence, C. P.; Skinner, J. L.; Fayer, M. D. *J. Chem. Phys.* **2004**, *121*, 12431−12446.

(38) Asbury, J. B.; Steinel, T.; Stromberg, C.; Corcelli, S. A.; Lawrence, C. P.; Skinner, J. L.; Fayer, M. D. *J. Phys. Chem. A* **2004**, *108*, 1107−1119.

(39) Loparo, J. J.; Roberts, S. T.; Tokmakoff, A. *J. Chem. Phys.* **2006**, *125*, 194521.

(40) Park, S.; Fayer, M. D. *Proc. Natl. Acad. Sci. U. S. A.* **2007**, *104*, 16731−16738.

(41) Yuan, R. F.; Yan, C.; Tamimi, A.; Fayer, M. D. *J. Phys. Chem. B* **2015**, *119*, 13407−13415.

(42) Hamm, P.; Lim, M.; Hochstrasser, R. M. *Phys. Rev. Lett.* **1998**, *81*, 5326−5329.

(43) King, J. T.; Kubarych, K. J. *J. Am. Chem. Soc.* **2012**, *134*, 18705−18712.

(44) Osborne, D. G.; Dunbar, J. A.; Lapping, J. G.; White, A. M.; Kubarych, K. J. *J. Phys. Chem. B* **2013**, *117*, 15407−15414.

(45) Laage, D.; Hynes, J. T. *Proc. Natl. Acad. Sci. U. S. A.* **2007**, *104*, 11167−11172.

(46) Sterpone, F.; Stirnemann, G.; Laage, D. *J. Am. Chem. Soc.* **2012**, *134*, 4116−4119.

(47) Yan, C.; Yuan, R. F.; Nishida, J.; Fayer, M. D. *J. Phys. Chem. C* **2015**, *119*, 16811−16823.

(48) Oudenhoven, T. A.; Joo, Y.; Laaser, J. E.; Gopalan, P.; Zanni, M. T. *J. Chem. Phys.* **2015**, *142*, 212449.

(49) Kwak, K.; Zheng, J.; Cang, H.; Fayer, M. D. *J. Phys. Chem. B* **2006**, *110*, 19998−20013.

(50) Kraack, J. P.; Frei, A.; Alberto, R.; Hamm, P. *J. Phys. Chem. Lett.* **2017**, *8*, 2489−2495.

(51) Rosenfeld, D. E.; Nishida, J.; Yan, C.; Gengeliczki, Z.; Smith, B. J.; Fayer, M. D. *J. Phys. Chem. C* **2012**, *116*, 23428−23440.

(52) Stine, K. J. *Microsc. Res. Tech.* **1994**, *27*, 439−450.

(53) Möhwald, H. *Annu. Rev. Phys. Chem.* **1990**, *41*, 441−476.

(54) Roberts, S. T.; Ramasesha, K.; Tokmakoff, A. *Acc. Chem. Res.* **2009**, *42*, 1239−1249.

(55) Cochran, R. E.; Ryder, O. S.; Grassian, V. H.; Prather, K. A. *Acc. Chem. Res.* **2017**, *50*, 599−604.